

# Porphyrin–Ryleneimide Hybrids: Tuning of Visible and Near-Infrared Absorption by Chromophore Desymmetrization

Sunit Kumar, Yogesh Kumar Maurya, Seongsoo Kang, Piotr Chmielewski, Tadeusz Lis, Joanna Cybińska, Dongho Kim,\* and Marcin Stępien\*



Cite This: *Org. Lett.* 2020, 22, 7202–7207



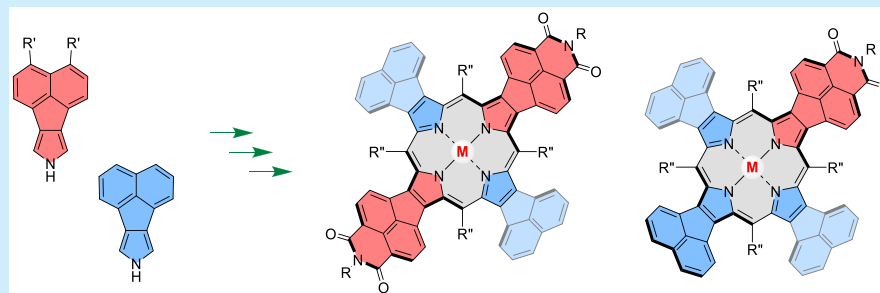
Read Online

ACCESS |

Metrics & More

Article Recommendations

Supporting Information



**ABSTRACT:** Unsymmetrically fused porphyrins containing one or two naphthalimide subunits were prepared in modular syntheses relying on electron-rich and electron-poor pyrrole building blocks. These new chromophores show progressive changes in their electron-deficient character, while retaining comparably small optical and electrochemical band gaps. The intrinsic curvature and extended optical absorption of these systems make them of interest as mono- and difunctional components of multichromophoric assemblies.

Ryleneimides, most notably perylenediimides (PDIs), are one of the most important classes of organic dyes, with an exceptional scope of industrial and research applications.<sup>1–5</sup> Their electronic and self-assembly properties can be tuned by homologation of the rylene backbone,<sup>3</sup> modification of imide functionalities,<sup>6</sup> peripheral substitution,<sup>1</sup> and ring fusion.<sup>7–9</sup> Hybridization of ryleneimides with nonbenzenoid and heterocyclic moieties provides a versatile though still relatively unexplored route to structurally unique functional dyes. In one general strategy,<sup>9,10</sup> tandem Pd-catalyzed couplings have been used for synthesis of ryleneimide-fused indenes,<sup>11</sup> azulenes,<sup>12</sup> corannulenes,<sup>13,14</sup> and heteroaromatics.<sup>15</sup> Our group has employed naphthaleneimide-fused pyrrole building blocks<sup>16</sup> for modular synthesis of electron-deficient porphyrins,<sup>16</sup> azacoronenes,<sup>17–19</sup> bipyrrroles,<sup>20</sup> and polymers.<sup>21</sup> This approach has so far yielded symmetrically fused A<sub>4</sub> porphyrins (**Scheme 1**), containing naphthalenediamide (NDA-fused, **1a**–H<sub>2</sub>) or naphthalenemonoimide acceptor units (NMI-fused, **1b**–H<sub>2</sub>), which have been explored as multielectron acceptors<sup>16</sup> and functional dyes.<sup>22</sup>

The electronic characteristics of such porphyrins can be tailored by juxtaposition of donor (D) and acceptor (A) units fused to the macrocyclic core (**Scheme 1**). In particular, we envisaged that the optical band gaps, absorption profiles, and redox properties of such mixed D–A porphyrins might be affected not only by the ratio of D and A subunits but also by the symmetry of the chromophore.<sup>23–27</sup> Systems containing

imide functionalities are highly attractive as components for multichromophoric systems obtainable by covalent or supramolecular assembly. For instance, donor BODIPY dyes attached radially to A<sub>4</sub>-type porphyrins via N-imide substituents yield efficient energy transfer according to the Förster mechanism.<sup>28</sup> The presence of four functionalization sites in the A<sub>4</sub> systems is however unsuitable for construction of unbranched architectures, notably linear and cyclic chromophore arrays. In this regard, D–A porphyrins containing fewer imide functionalities are essential as mono- or bifunctional building blocks, simultaneously analogous to ryleneimides, and other unsymmetrically functionalized porphyrins.<sup>29–32</sup>

With these possibilities in mind, we now developed synthetic routes to two classes of low-symmetry chromophores: tD<sub>2</sub>A<sub>2</sub> and DA<sub>3</sub>, which can be viewed as porphyrin-hybridized equivalents of rylene diimides and monoimides, respectively. In principle, mixed donor–acceptor porphyrins, namely tD<sub>2</sub>A<sub>2</sub>, D<sub>3</sub>A, DA<sub>3</sub>, and cD<sub>2</sub>A<sub>2</sub>, are obtainable in a three-component cross-condensation of two different pyrroles and an aldehyde.<sup>33</sup>

Received: July 30, 2020

Published: August 28, 2020



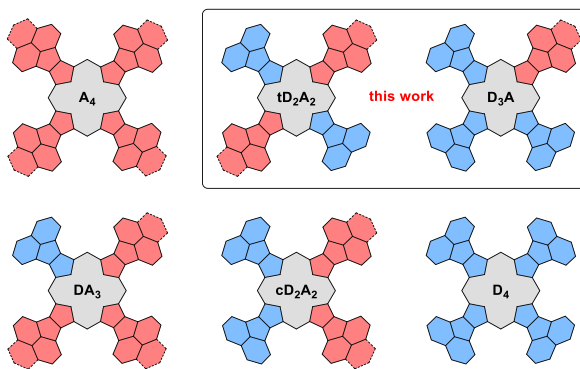
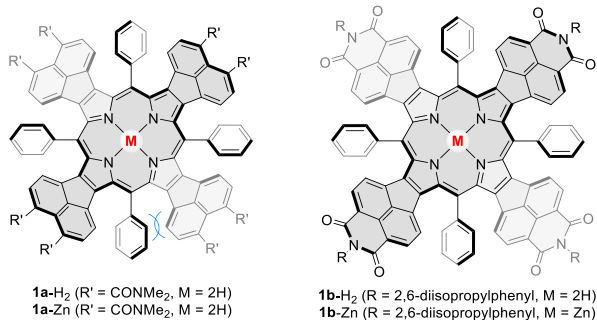
ACS Publications

© 2020 American Chemical Society

7202

<https://dx.doi.org/10.1021/acs.orglett.0c02544>  
*Org. Lett.* 2020, 22, 7202–7207

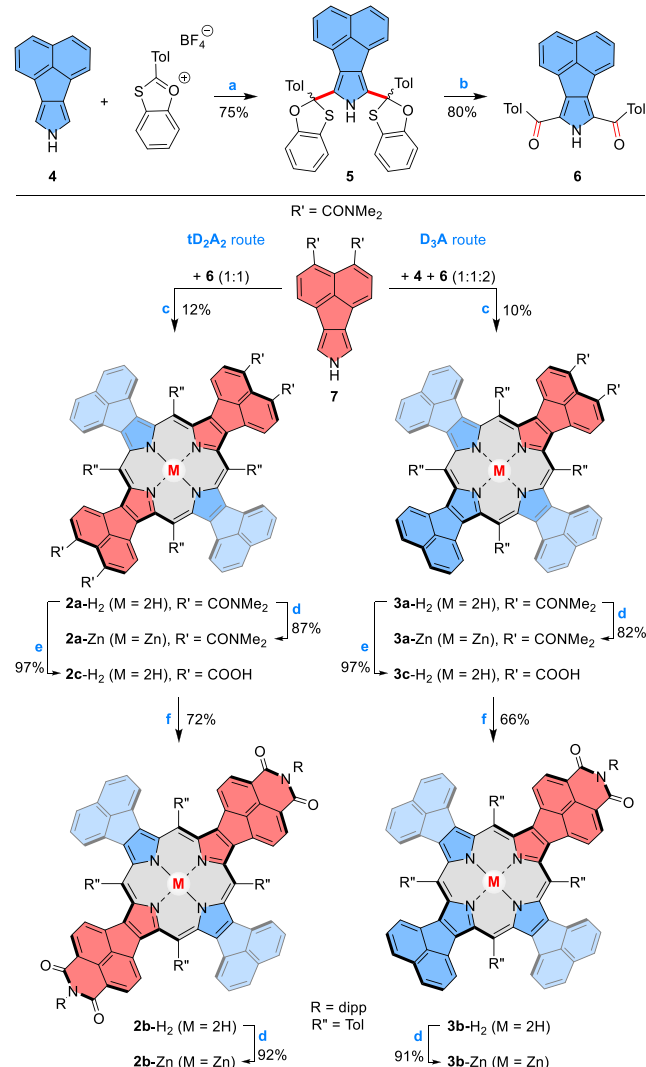
**Scheme 1. Donor–Acceptor Porphyrins with Mixed Ring Fusion Patterns**



Such a strategy is generally unselective and may fail if the reactivity of the two pyrroles is significantly different. To circumvent these problems, we used a multistep approach shown in **Scheme 2**. First, the reaction of acenaphthopyrrole **4**<sup>34</sup> and 2-tolyl 1,3-benzoxathiolium tetrafluoroborate<sup>35,36</sup> afforded the masked diketone **5**, which was hydrolyzed to yield the diacyl pyrrole **6**. The latter intermediate was reduced with  $\text{NaBH}_4$  in  $\text{THF}/\text{CH}_3\text{OH}$ , and the resulting crude acenaphthopyrrole dicarbinol was condensed with 1 equiv of diamide pyrrole **7**.<sup>16</sup> Following column chromatography, the desired **tD<sub>2</sub>A<sub>2</sub>** porphyrin **2a-H<sub>2</sub>** was isolated in a 12% yield. Similarly, a cross-condensation of **7**, **4**, and reduced **6** in a 1:1:2 molar ratio furnished the **D<sub>3</sub>A**-type porphyrin **3a-H<sub>2</sub>** as the major product. **2a-H<sub>2</sub>** and **3a-H<sub>2</sub>** were transformed into the respective imide derivatives **2b-H<sub>2</sub>** and **3b-H<sub>2</sub>** using a two-step procedure consisting of acid hydrolysis followed by imidization with 2,6-diisopropylaniline. Finally, the four new porphyrins were metallated with zinc(II) acetate, yielding the corresponding complexes, **2a-Zn**, **3a-Zn**, **2b-Zn**, and **3b-Zn**. All the compounds were thoroughly characterized by HR-MS as well as 1D and 2D NMR spectroscopy, and the structures of porphyrins **2b-H<sub>2</sub>**/**3b-H<sub>2</sub>** were confirmed X-ray crystallography.

The free bases **2b-H<sub>2</sub>** and **3b-H<sub>2</sub>** were characterized crystallographically in the solid state (Figure 1). In each case, a trans tautomer was observed, with the NH protons located on the more electron-rich pair of pyrroles.<sup>37</sup> Each macrocycle showed a pronounced saddle-shaped distortion of the aromatic surface. This characteristic feature is caused by the steric congestion between the outer naphthalene moieties and the *meso*-tolyl substituents, and precludes stacking interactions between the porphyrin  $\pi$  surfaces. The dihedral angles between opposite naphthalene subunits in **2b-H<sub>2</sub>** are  $117.5^\circ$  (NMI/NMI) and  $109.1^\circ$  (naph/naph, cf. Figure 1), producing a similar level of curvature to that previously

**Scheme 2. Synthesis of Mixed Donor–Acceptor Porphyrins<sup>a</sup>**



<sup>a</sup>Reagents and conditions: (a) pyridine,  $\text{CH}_3\text{CN}/\text{CHCl}_3$  (1:1 v/v), 1 h; (b)  $\text{HgO}$ ,  $\text{HBF}_4$ ,  $\text{THF}$ , 5 h; (c) (i) **6**,  $\text{NaBH}_4$ ,  $\text{THF}/\text{MeOH}$  (3:1 v/v), 2 h, (ii) **7** (4, for **3a-H<sub>2</sub>**), *p*-TSA,  $\text{CHCl}_3/\text{MeOH}$  (100:1 v/v), 1 h; (iii) DDQ, 2 h; (d)  $\text{Zn}(\text{OAc})_2 \cdot 2\text{H}_2\text{O}$ ,  $\text{CHCl}_3/\text{MeOH}$  (3:1 v/v); (e)  $\text{HCl}$ , reflux, 24 h; (f) 2,6-diisopropylaniline, acetic acid, 20 h, reflux. Tol = *p*-tolyl, dipp = 2,6-diisopropylphenyl.

observed for **1b-H<sub>2</sub>**. Remarkably, the corresponding angles in **3b-H<sub>2</sub>** are drastically different ( $90.2^\circ$  and  $128.8^\circ$  for naph/NMI and naph/naph, respectively). In DFT-optimized geometries of **2b-H<sub>2</sub>** and **3b-H<sub>2</sub>** (Table S14), the dihedrals involving NMI units are very similar ( $98^\circ$ – $99^\circ$ ), indicating that the geometry difference observed in the solid state is caused by crystal packing and is most likely absent in solution. In the crystal, the surface of **3b-H<sub>2</sub>** apparently wraps around the unique dipp group of a neighboring molecule, and this interaction is propagated along one direction, to produce densely packed ribbons stabilized by multiple  $\text{CH}\cdots\pi$  interactions (Figure 1D). A similar type of interaction between dipp groups and aromatic surfaces is found in the crystal of **2b-H<sub>2</sub>** (Figure 1C); however, the resulting pattern is less dense and produces no additional distortion of the aromatic core. As a consequence, the latter structure is more highly solvated (**2b-H<sub>2</sub>**· $1.75\text{C}_6\text{H}_{14}\cdot 8.8\text{CHCl}_3$  vs **3b-H<sub>2</sub>**· $2.8\text{C}_6\text{H}_{14}\cdot 3.1\text{CHCl}_3$ ), sim-

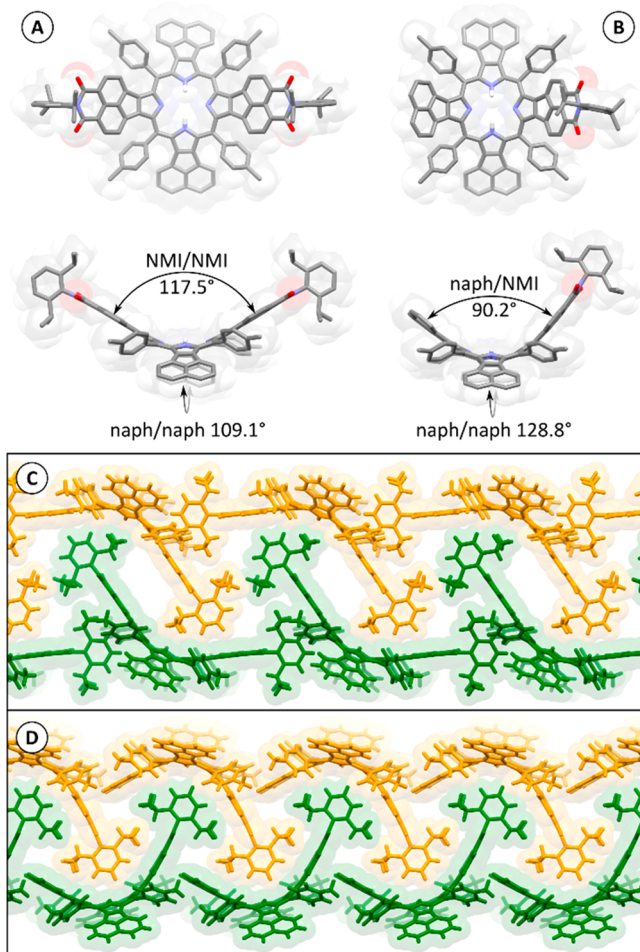


**Figure 1.** Molecular structures and packing diagrams of **2b**-H<sub>2</sub> (A and C) and **3b**-H<sub>2</sub> (B and D) obtained in X-ray crystallographic analyses. C-bound hydrogen atoms (A and B) and solvent molecules (A–D) are omitted for clarity. Interplanar angles (A and B) were calculated between C<sub>10</sub> planes of naphthalene (naph) and naphthalenemonoimide (NMI) subunits.

ilarly to the previously reported structures of **1b**-H<sub>2</sub> and **1b**-Zn.<sup>16</sup>

Steady-state absorption spectra of the newly synthesized tD<sub>2</sub>A<sub>2</sub> and D<sub>3</sub>A porphyrins contain an intense Soret-like band at ca. 600 nm and a series of Q bands extending into the near-infrared (Figure 2 and Tables 1 and S1). Zinc complexes were characterized in the presence of excess pyridine to suppress aggregation previously observed for amide-bearing derivatives.<sup>16</sup> For the NDA systems, the difference between the absorption profiles of tD<sub>2</sub>A<sub>2</sub> and D<sub>3</sub>A-type chromophores (i.e., **2a**-M vs **3a**-M) is relatively insignificant. In particular, the di-NDA free base **2a**-H<sub>2</sub> shows a Soret band at 568 nm and three Q bands at 639, 709, 778 nm, whereas, in mono-NDA porphyrin **3a**-H<sub>2</sub>, the Soret band is slightly blue-shifted to 559 nm, whereas the lowest-energy Q-band shows a red shift to 803 nm. In fact these spectra are similar to those of **1a**-H<sub>2</sub><sup>16</sup> and the corresponding D<sub>4</sub> system,<sup>38</sup> implying a relatively weak interaction between the π system and the twisted dimethylaminocarbonyl substituents. In contrast, the optical properties of **2b**-M and **3b**-M are significantly perturbed by the fusion of NMI subunits. All systems show extended NIR bands, with the absorption onset in each case approaching 1000 nm. Interestingly, in spite of the smaller number of electron-

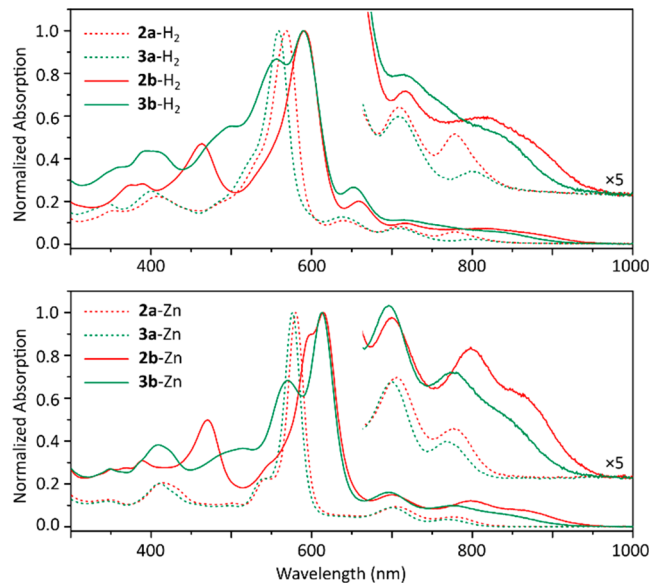


**Figure 2.** Electronic absorption spectra of **2a**-M, **2b**-M, **3a**-M, and **3b**-M (5 μM concentration; M = 2H in dichloromethane, M = Zn in toluene + 1% pyridine).

**Table 1. Photophysical and Electrochemical Properties of Compounds **2a**-M, **2b**-M, **3a**-M, and **3b**-M (M = 2H, Zn)<sup>a,b</sup>**

Species	Q <sub>1</sub> (Soret) [nm] <sup>b</sup>	λ <sub>max</sub> <sup>em</sup> [nm] <sup>c</sup>	E <sub>ox1</sub> <sup>d</sup> [V]	E <sub>red1</sub> <sup>d</sup> [V]	ΔE <sup>d</sup> [V]
<b>2a</b> -H <sub>2</sub>	778 (568)	837	0.26	-1.34	1.60
<b>2b</b> -H <sub>2</sub>	823 (590)	956	0.36	-1.08	1.44
<b>3a</b> -H <sub>2</sub>	803 (559)	833	0.25	-1.36	1.61
<b>3b</b> -H <sub>2</sub>	834 (590)	950	0.30	-1.14	1.44
<b>1a</b> -Zn	775 (583)	806	0.22	-1.42	1.64
<b>1b</b> -Zn	838 (632)	893	0.34	-1.00	1.34
<b>2a</b> -Zn	780 (579)	810	0.08	-1.63	1.71
<b>2b</b> -Zn	864 (614)	930	0.24	-1.19	1.43
<b>3a</b> -Zn	768 (577)	815	0.11	-1.64	1.75
<b>3b</b> -Zn	852 (613)	920	0.18	-1.22	1.40

<sup>a</sup>Data in dichloromethane. For additional data, see the Supporting Information. <sup>b</sup>Maximum absorption for the lowest-energy Q-band and for the most intense Soret band. Data for the previously reported<sup>16</sup> **1a**-Zn and **1b**-Zn are provided for comparison.

<sup>c</sup>Fluorescence emission maximum. <sup>d</sup>First oxidation and reduction potentials (relative to Fc/Fc<sup>+</sup>) and the electrochemical band gap.

withdrawing NMI moieties, the band gaps of all these systems are apparently reduced relative to that of **1b**-M.<sup>16</sup> This observation is further confirmed by the positions of emission maxima of the weakly fluorescent complexes **2b**-Zn and **3b**-Zn (930 and 920 nm, respectively, Figures S7 and S8), which are both red-shifted relative to **1b**-Zn<sup>16</sup> (893 nm). The mono-NMI systems **3b**-M have somewhat larger optical gaps than their di-NMI analogues.

Interestingly, on going from **1b**-M, through **2b**-M, to **3b**-M, gradual reduction of molecular symmetry produces increasingly broadened absorption in the visible (Soret-like) region of the absorption spectrum, which is a beneficial characteristic for potential light-harvesting applications. Moreover, symmetry effects have an influence on excited-state population dynamics of **2b**-Zn and **3b**-Zn, which were investigated using femtosecond transient absorption spectroscopy. Upon photoexcitation, **2b**-Zn and **3b**-Zn showed singlet state lifetimes of

460 and 230 ps followed by infinite residues contributed by the intersystem crossing processes to the triplet state (Figures S9 and S10). Thus, the excited singlet states of **2b**-Zn and **3b**-Zn are quenched 4 to 6 times faster than observed for **1b**-Zn,<sup>28</sup> indicating a faster deactivation of the excited singlet state in the asymmetrical structures.

In dichloromethane or THF solutions, **2b**-M and **3b**-M ( $M = 2H, Zn$ ) showed up to two chemically reversible oxidations, followed by additional nonreversible events at higher potentials (Tables 1 and S2 and Figures S12 and S13). The monoimides (**3b**-M) are easier to oxidize and more difficult to reduce than the diimides (**2b**-M), in line with the more electron-deficient character of the latter derivatives. Interestingly, however, electrochemical band gaps of corresponding mono- and diimide species are nearly identical. Similarly to their tetra-NMI congeners,<sup>16</sup> the imide-fused systems show multiple reduction events at relatively high potentials. NDA-fused analogues **2a**-M and **3a**-M showed qualitatively similar electrochemical behavior, with larger band gaps than their NMI analogues.

Kohn–Sham molecular orbitals (MOs), calculated for NMI-fused systems **1b**'-M, **2b**'-M, and **3b**'-M and their imide-free parent **8b**'-M ( $M = 2H, Zn$ ; Figure 3), show progressive lowering of occupied and virtual energy levels when the

number of NMI units is increased. Mono-NMI systems **3b**'-M have significantly smaller electronic band gaps than their **8b**'-M counterparts (by 0.2–0.25 eV). Remarkably, the band gaps of **2b**'-M and **1b**'-M do not decrease uniformly with the increasing number of NMI groups. Instead, they vary over a relatively small range of energies and, in fact, the smallest gaps are predicted for the di-NMI systems **2b**'-M rather than for **1b**'-M. *meso*-Tol substituents are predicted to produce a further small decrease of the optical band gap relative to *meso*-Ph systems (Table S4), explaining why **2b**-M and **3b**-M have smaller optical gaps than the Ph-substituted **1b**-M. Absorption spectra simulated for the fully substituted **2b**-Zn and **3b**-Zn using time-dependent DFT are consistent with experimental data, reproducing positions of Q and Soret bands (Figure 3).

The porphyrin–ryleneimide hybrids described herein reveal nontrivial relationships between the electronic properties of the  $\pi$  system and the placement of fused acceptor units around the porphyrin core. The electron-deficient character of these molecules is gradually enhanced with the increasing number of acceptors; however, the electronic band gap is significantly reduced only by introduction of the first NMI unit, but it is just moderately affected when further NMI moieties are added. Interestingly, the smallest gap is observed for the tD<sub>2</sub>A<sub>2</sub> porphyrin, which is highly attractive as an NIR-absorbing, intrinsically curved analogue of perylenediimide. In subsequent work, we plan to employ this new chromophore and its monoimide congener as components in supramolecular and covalently linked energy- and charge-transfer systems.

## ASSOCIATED CONTENT

### Supporting Information

The Supporting Information is available free of charge at <https://pubs.acs.org/doi/10.1021/acs.orglett.0c02544>.

Synthetic, crystallographic, and spectroscopic details, computational data (PDF)

Cartesian coordinates in the PDB format (ZIP)

## Accession Codes

CCDC 2015790–2015791 contain the supplementary crystallographic data for this paper. These data can be obtained free of charge via [www.ccdc.cam.ac.uk/data\\_request/cif](http://www.ccdc.cam.ac.uk/data_request/cif), or by emailing [data\\_request@ccdc.cam.ac.uk](mailto:data_request@ccdc.cam.ac.uk), or by contacting The Cambridge Crystallographic Data Centre, 12 Union Road, Cambridge CB2 1EZ, UK; fax: +44 1223 336033.

## AUTHOR INFORMATION

### Corresponding Authors

**Dongho Kim** – Department of Chemistry and Spectroscopy Laboratory for Functional  $\pi$ -Electronic Systems, Yonsei University, Seoul 03722, Korea; [orcid.org/0000-0001-8668-2644](https://orcid.org/0000-0001-8668-2644); Email: [marcin.stepien@chem.uni.wroc.pl](mailto:marcin.stepien@chem.uni.wroc.pl)

**Marcin Stępien** – Wydział Chemiczny, Uniwersytet Wrocławski, 50-383 Wrocław, Poland; [orcid.org/0000-0002-4670-8093](https://orcid.org/0000-0002-4670-8093); Email: [dongho@yonsei.ac.kr](mailto:dongho@yonsei.ac.kr)

### Authors

**Sunit Kumar** – Wydział Chemiczny, Uniwersytet Wrocławski, 50-383 Wrocław, Poland

**Yogesh Kumar Maurya** – Wydział Chemiczny, Uniwersytet Wrocławski, 50-383 Wrocław, Poland

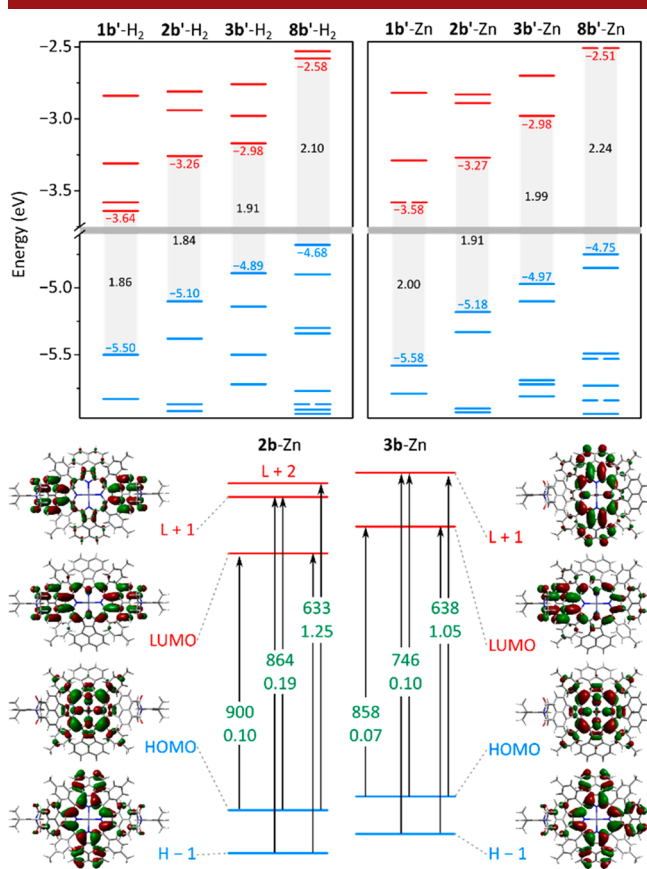


**Figure 3.** Electronic structure calculations for homologous NMI-fused porphyrins ( $M = 2H$ ) and zinc porphyrins ( $M = Zn$ , B3LYP/6-31G(d,p), DCM solvation included for TD-DFT). Top: Kohn–Sham frontier MO levels for **1b**'-M ( $R = H$ ), **2b**'-M and **3b**'-M ( $R = H, R'' = Ph$ ), and **8b**'-M ( $D_4$ -type porphyrin with *meso*-phenyl substituents). Bottom: MO amplitudes and key TD-DFT transitions for **2b**-Zn and **3b**-Zn. Transition energies (nm) and oscillator strengths are shown in green.

**Seongsoo Kang** — Department of Chemistry and Spectroscopy  
Laboratory for Functional  $\pi$ -Electronic Systems, Yonsei  
University, Seoul 03722, Korea

**Piotr Chmielewski** — Wydział Chemii, Uniwersytet Wrocławski,  
50-383 Wrocław, Poland; orcid.org/0000-0002-2548-  
6110

**Tadeusz Lis** — Wydział Chemii, Uniwersytet Wrocławski, 50-  
383 Wrocław, Poland

**Joanna Cybińska** — Wydział Chemii, Uniwersytet Wrocławski,  
50-383 Wrocław, Poland; PORT — Polski Ośrodek Rozwoju  
Technologii, 54-066 Wrocław, Poland

Complete contact information is available at:

<https://pubs.acs.org/10.1021/acs.orglett.0c02544>

## Notes

The authors declare no competing financial interest.

## ACKNOWLEDGMENTS

Financial support from the Foundation for Polish Science (TEAM POIR.04.04.00.00-SBF1/17-00, M.S.) is gratefully acknowledged. Quantum-chemical calculations were performed in the Wrocław Center for Networking and Supercomputing. The work at Yonsei University was supported the National Research Foundation of Korea (NRF) grant funded by the Korea government (MEST) (NRF-2016R1E1A1A01943379).

## REFERENCES

- (1) Suraru, S.-L.; Würthner, F. Strategies for the Synthesis of Functional Naphthalene Diimides. *Angew. Chem., Int. Ed.* **2014**, *53* (29), 7428–7448.
- (2) Würthner, F.; Saha-Möller, C. R.; Fimmel, B.; Ogi, S.; Leowanawat, P.; Schmidt, D. Perylene Bisimide Dye Assemblies as Archetype Functional Supramolecular Materials. *Chem. Rev.* **2016**, *116* (3), 962–1052.
- (3) Chen, L.; Li, C.; Müllen, K. Beyond Perylene Diimides: Synthesis, Assembly and Function of Higher Rylene Chromophores. *J. Mater. Chem. C* **2014**, *2* (11), 1938–1956.
- (4) Al Kobaisi, M.; Bhosale, S. V.; Latham, K.; Raynor, A. M.; Bhosale, S. V. Functional Naphthalene Diimides: Synthesis, Properties, and Applications. *Chem. Rev.* **2016**, *116* (19), 11685–11796.
- (5) Nowak-Krół, A.; Shoyama, K.; Stolte, M.; Würthner, F. Naphthalene and Perylene Diimides – Better Alternatives to Fullerenes for Organic Electronics? *Chem. Commun.* **2018**, *54* (98), 13763–13772.
- (6) Jänsch, D.; Li, C.; Chen, L.; Wagner, M.; Müllen, K. Versatile Colorant Syntheses by Multiple Condensations of Acetyl Anilines with Perylene Anhydrides. *Angew. Chem., Int. Ed.* **2015**, *54* (7), 2285–2289.
- (7) Li, C.; Lin, Z.; Li, Y.; Wang, Z. Synthesis and Applications of  $\pi$ -Extended Naphthalene Diimides. *Chem. Rec.* **2016**, *16* (2), 873–885.
- (8) Stępień, M.; Gońska, E.; Żyła, M.; Sprutta, N. Heterocyclic Nanographenes and Other Polycyclic Heteroaromatic Compounds: Synthetic Routes, Properties, and Applications. *Chem. Rev.* **2017**, *117* (4), 3479–3716.
- (9) Zhylitskaya, H.; Stępień, M. Carbocyclization Approaches to Electron-Deficient Nanographenes and Their Analogues. *Org. Chem. Front.* **2018**, *5* (15), 2395–2414.
- (10) Seifert, S.; Shoyama, K.; Schmidt, D.; Würthner, F. An Electron-Poor C<sub>64</sub> Nanographene by Palladium-Catalyzed Cascade C–C Bond Formation: One-Pot Synthesis and Single-Crystal Structure Analysis. *Angew. Chem., Int. Ed.* **2016**, *55* (22), 6390–6395.
- (11) Seifert, S.; Schmidt, D.; Shoyama, K.; Würthner, F. Base-Selective Five- versus Six-Membered Ring Annulation in Palladium-Catalyzed C–C Coupling Cascade Reactions: New Access to Electron-Poor Polycyclic Aromatic Dicarboximides. *Angew. Chem., Int. Ed.* **2017**, *56* (26), 7595–7600.
- (12) Pigulski, B.; Shoyama, K.; Würthner, F. NIR-Absorbing  $\pi$ -Extended Azulene: Non-Alternant Isomer of Terrylene Bisimide. *Angew. Chem., Int. Ed.* **2020**. DOI: 10.1002/anie.202005376.
- (13) Shoyama, K.; Würthner, F. Synthesis of a Carbon Nanocone by Cascade Annulation. *J. Am. Chem. Soc.* **2019**, *141* (33), 13008–13012.
- (14) Renner, R.; Stolte, M.; Würthner, F. Self-Assembly of Bowl-Shaped Naphthalimide-Annulated Corannulene. *ChemistryOpen* **2020**, *9* (1), 32–39.
- (15) Shoyama, K.; Mahl, M.; Seifert, S.; Würthner, F. A General Synthetic Route to Polycyclic Aromatic Dicarboximides by Palladium-Catalyzed Annulation Reaction. *J. Org. Chem.* **2018**, *83* (10), 5339–5346.
- (16) Zhylitskaya, H.; Cybińska, J.; Chmielewski, P.; Lis, T.; Stępień, M. Bandgap Engineering in  $\pi$ -Extended Pyrroles. a Modular Approach to Electron-Deficient Chromophores with Multi-Redox Activity. *J. Am. Chem. Soc.* **2016**, *138* (35), 11390–11398.
- (17) Żyła-Karwowska, M.; Zhylitskaya, H.; Cybińska, J.; Lis, T.; Chmielewski, P. J.; Stępień, M. An Electron-Deficient Azacoronene Obtained by Radial  $\pi$  Extension. *Angew. Chem., Int. Ed.* **2016**, *55* (47), 14658–14662.
- (18) Navakouski, M.; Zhylitskaya, H.; Chmielewski, P. J.; Lis, T.; Cybińska, J.; Stępień, M. Stereocontrolled Synthesis of Chiral Heteroaromatic Propellers with Small Optical Bandgaps. *Angew. Chem., Int. Ed.* **2019**, *58* (15), 4929–4933.
- (19) Moshniah, L.; Żyła-Karwowska, M.; Chmielewski, P. J.; Lis, T.; Cybińska, J.; Gońska, E.; Oschwald, J.; Drewello, T.; Rivero, S. M.; Casado, J.; Stępień, M. Aromatic Nanosandwich Obtained by  $\sigma$ -Dimerization of a Nanographenoid  $\pi$ -Radical. *J. Am. Chem. Soc.* **2020**, *142* (7), 3626–3635.
- (20) Żyła-Karwowska, M.; Moshniah, L.; Hong, Y.; Zhylitskaya, H.; Cybińska, J.; Chmielewski, P. J.; Lis, T.; Kim, D.; Stępień, M. Electron-Deficient Bipyrrole Boomerangs: Bright Fluorophores Obtained via Double C–H Bond Activation. *Chem. - Eur. J.* **2018**, *24* (29), 7525–7530.
- (21) Czichy, M.; Zhylitskaya, H.; Zassowski, P.; Navakouski, M.; Chulkin, P.; Janasik, P.; Lapkowski, M.; Stępień, M. Electrochemical Polymerization of Pyrrole–Perimidine Hybrids: Low-Bandgap Materials with High n-Doping Activity. *J. Phys. Chem. C* **2020**, *124*, 14350.
- (22) Galstyan, A.; Maurya, Y. K.; Zhylitskaya, H.; Bae, Y. J.; Wu, Y. L.; Wasielewski, M. R.; Lis, T.; Dobrindt, U.; Stępień, M.  $\pi$ -Extended Donor–Acceptor Porphyrins and Metalloporphyrins for Antimicrobial Photodynamic Inactivation. *Chem. - Eur. J.* **2020**, *26* (37), 8262–8266.
- (23) Imahori, H.; Umeyama, T.; Ito, S. Large  $\pi$ -Aromatic Molecules as Potential Sensitizers for Highly Efficient Dye-Sensitized Solar Cells. *Acc. Chem. Res.* **2009**, *42* (11), 1809–1818.
- (24) Kurotobi, K.; Toude, Y.; Kawamoto, K.; Fujimori, Y.; Ito, S.; Chabera, P.; Sundström, V.; Imahori, H. Highly Asymmetrical Porphyrins with Enhanced Push–Pull Character for Dye-Sensitized Solar Cells. *Chem. - Eur. J.* **2013**, *19* (50), 17075–17081.
- (25) Rathi, P.; Butcher, R.; Sankar, M. Unsymmetrical Nonplanar ‘Push–Pull’  $\beta$ -Octasubstituted Porphyrins: Facile Synthesis, Structural, Photophysical and Electrochemical Redox Properties. *Dalton Trans* **2019**, *48* (40), 15002–15011.
- (26) Sekaran, B.; Jang, Y.; Misra, R.; D’Souza, F. Push–Pull Porphyrins via  $\beta$ -Pyrrole Functionalization: Evidence of Excited State Events Leading to High-Potential Charge-Separated States. *Chem. - Eur. J.* **2019**, *25* (56), 12991–13001.
- (27) Rathi, P.; Ekta; Kumar, S.; Banerjee, D.; Soma, V. R.; Sankar, M. Unsymmetrical  $\beta$ -Functionalized ‘Push–Pull’ Porphyrins: Synthesis and Photophysical, Electrochemical and Nonlinear Optical Properties. *Dalton Trans* **2020**, *49* (10), 3198–3208.
- (28) Janiga, E.; Kim, G.; Chmielewski, P. J.; Lis, T.; Kim, D.; Stępień, M. Porphyrin-Ryleneimide Hybrids: Low-Bandgap Acceptors

in Energy-Transfer Cassettes. *Chem. - Asian J.* **2020**. DOI: 10.1002/asia.202000762.

(29) Lindsey, J. S. Synthetic Routes to Meso -Patterned Porphyrins. *Acc. Chem. Res.* **2010**, 43 (2), 300–311.

(30) Vicente, M.; Smith, K. Syntheses and Functionalizations of Porphyrin Macrocycles. *Curr. Org. Synth.* **2014**, 11 (1), 3–28.

(31) Tanaka, T.; Osuka, A. Conjugated Porphyrin Arrays: Synthesis, Properties and Applications for Functional Materials. *Chem. Soc. Rev.* **2015**, 44 (4), 943–969.

(32) Hiroto, S.; Miyake, Y.; Shinokubo, H. Synthesis and Functionalization of Porphyrins through Organometallic Methodologies. *Chem. Rev.* **2017**, 117 (4), 2910–3043.

(33) Hoshino, A.; Ohgo, Y.; Nakamura, M. Synthesis and Inversion Barriers of Undeca- and Dodeca-Substituted Saddle Shaped Porphyrin Complexes. *Tetrahedron Lett.* **2005**, 46 (30), 4961–4964.

(34) Spence, J. D.; Lash, T. D. Porphyrins with Exocyclic Rings. 14. Synthesis of Tetraacenaphthoporphyrins, a New Family of Highly Conjugated Porphyrins with Record-Breaking Long-Wavelength Electronic Absorptions. *J. Org. Chem.* **2000**, 65 (5), 1530–1539.

(35) Barbero, M.; Cadamuro, S.; Degani, I.; Fochi, R.; Gatti, A.; Regondi, V. Useful Syntheses of 2-Substituted 1,3-Benzoxathiolium Tetrafluoroborates from Carboxylic Acids, Anhydrides, Esters and Trihalomethyl Compounds. *Synthesis* **1986**, 1986 (12), 1074–1076.

(36) Barbero, M.; Cadamuro, S.; Degani, I.; Fochi, R.; Gatti, A.; Regondi, V. Pentatomic Heteroaromatic Cations. 18. Acylation of Pyrrole and N-Methylpyrrole with 1,3-Benzoxathiolium Tetrafluoroborates. A High-Yield Method for the Synthesis of Diacylpyrroles. *J. Org. Chem.* **1988**, 53 (10), 2245–2250.

(37) Crossley, M. J.; Harding, M. M.; Sternhell, S. Tautomerism in 2-Substituted 5,10,15,20-Tetraphenylporphyrins. *J. Am. Chem. Soc.* **1986**, 108 (13), 3608–3613.

(38) Lash, T. D.; Chandrasekar, P. Synthesis of Tetraphenyltetraacenaphthoporphyrin: A New Highly Conjugated Porphyrin System with Remarkably Red-Shifted Electronic Absorption Spectra. *J. Am. Chem. Soc.* **1996**, 118 (36), 8767–8768.